HHS Public Access

Author manuscript

ACS Appl Nano Mater. Author manuscript; available in PMC 2020 September 29.

Published in final edited form as:

ACS Appl Nano Mater. 2018 April 27; 1(4): 1595–1602. doi:10.1021/acsanm.8b00069.

Tetrahedral (*T*) Closed-Shell Cluster of 29 Silver Atoms & 12 Lipoate Ligands, $[Ag_{29}(R\text{-}\alpha\text{-}LA)_{12}]^{(3-)}$: Antibacterial and Antifungal Activity

Priscilla Lopez[†], **Humberto H. Lara**[‡], **Sean M. Mullins**[†], **David M. Black**[†], **Heidi M. Ramsower**[†], **Marcos M. Alvarez**[*,†], **Tayler L. Williams**[§], **Xochitl Lopez-Lozano**[†], **Hans-Christian Weissker**[‖,⊥], **A. Patricio García**[#], **Ignacio L. Garzón**[#], **Borries Demeler**[§], **José Luis Lopez-Ribot**[‡], **Miguel José Yacamán**[†], **Robert L. Whetten**[*,†]

[†]Department of Physics & Astronomy, University of Texas, San Antonio, Texas 78249, United States

[‡]Department of Biology and South Texas Center for Emerging Infectious Diseases, University of Texas, San Antonio, Texas 78249, United States

[§]The University of Texas Health Science Center, San Antonio, Texas 78229, United States

[‖]Aix Marseille University, CNRS, CINaM UMR 7325, 13288 Marseille, France

[⊥]European Theoretical Spectroscopy Facility

[#]Instituto de Física, Universidad Nacional Autónoma de México, Apartado Postal 20-364, 01000 México D. F., México

Abstract

Here we report on the identification and applications of an aqueous 29-atom silver cluster stabilized with 12 lipoate ligands, i.e. $Ag_{29}(R\text{-}\alpha\text{–}LA)_{12}$ or (29,12), wherein R-α–LA = R-α-lipoic acid, a natural dithiolate. Its uniformity is checked by HPLC-ESI-MS and analytical ultracentrifugation, which confirms its small dimension (~3 nm hydrodynamic diameter). For the first time, this cluster has been detected intact via electrospray ionization mass spectrometry, allowing one to confirm its composition, its [3-] charge-state, and the 8-electron shell configuration of its metallic silver core. Its electronic structure and bonding, including T-symmetry and profound chirality in the outer shell, have been analyzed by DFT quantum-chemical calculations, starting from the known structure of a nonaqueous homologue. The cluster is effective against Methicillin-Resistant *Staphylococcus aureus* bacteria (MRSA) at a minimum inhibitory concentration (MIC) of 0.6 mg-Ag/mL. A preformed *Candida albicans* fungal biofilm, impermeable to other antifungal agents, was also inhibited by aqueous solutions of this cluster, in a dose–response manner, with a half-maximal inhibitory concentration (IC_{50}) of 0.94 mg-Ag/mL.

[*]**Corresponding Authors:** marcos.alvarez@utsa.edu., robert.whetten@utsa.edu.

Supporting Information

The Supporting Information is available free of charge on the ACS Publications website at DOI: 10.1021/acsanm.8b00069. Detailed methodology is provided for cluster synthesis, cluster purification, mass spectrometer and HPLC operational parameters, antibiotic assays, AUC analysis and results, AEM methods and analysis, and DFT theoretical calculation; structural coordinate files available upon request (PDF)

The authors declare no competing financial interest.

Scanning electron micrographs showed the post-treatment ultrastructural changes on both MRSA and C. *albicans* that are characteristic of those displayed after treatment by larger silver nanoparticles.

Graphical abstract

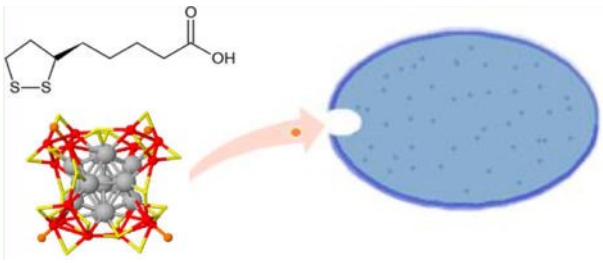

Keywords

silver clusters; lipoic acid; antibiotic; analytical ultracentrifugation; electrospray ionization mass spectrometry; Ag_{29}

1. INTRODUCTION

For centuries, silver has been used as a bactericidal agent in applications ranging from food storage to wound treatment; yet this practice over the years started to decrease with the discovery and use of organic antibiotics.[1–3] Recently, the interest in using silver as an antibacterial agent has increased due to the emergence of antibiotic-resistant strains of bacteria.[4–8] As of April 2017, the Center for Disease Control and Prevention has estimated that each year at least 2 million people in the United States alone become infected with an antibiotic resistant bacterium, leading to some 23 000 deaths caused by those infections.[4] Silver nanoparticles alone have been found to attach to the surface of the cell membrane of bacteria and disturb its functionality; they also exhibit the ability to penetrate the membrane.[3,7,9–14] The smallest silver particles, such as the cluster compound investigated herein, of ~3 nm hydrodynamic diameter, offer the additional advantage of not exhibiting long-term absorption in the body.[15,16]

Recently, several groups have reported on the special stability (high yield) and optical properties relating to silver clusters that comprise 29 Ag atoms and 12 ligands.[17–21] A water-soluble variant, stabilized with lipoate (LA) ligands,[18–20] has been tentatively identified as $Ag_{29}LA_{12}$ by analogy to the hydrophobic homologue determined by Abdul-Halim et al.[21] (R)-Alpha lipoic acid (R-α-LA) is a naturally occurring dithiol that exhibits diverse biomedical effects ranging from anti-inflammatory to powerful antioxidant protection.[22,23] R-α-LA plays a significant role in energy production.[24] For these reasons, it has also found extensive use as a template for therapeutic drug development.[25] The $Ag_{29}LA_{12}$ thus exploits both the biological activity of the silver core and the biocompatibility of the R-α-LA ligand, which motivated us to test whether the cluster will be an effective antimicrobial agent. We will present evidence that the cluster is indeed an antibiotic agent after first discussing its

compositional assignment via mass spectrometry, its electronic structure and bonding via DFT computations, and its hydrodynamic size estimate via analytical ultracentrifugation.

2. EXPERIMENTAL METHODS

2.1. Synthesis and LC/MS Characterization.

The $Ag_{29}(LA)_{12}$ clusters were prepared using the protocol described by van der Linden et al.[19] scaled 10-fold. The raw product was purified by sequential washing with acetone followed by extraction with methanol, as detailed in the Supporting Information, and analyzed in a Bruker micrOTOF time-of-flight mass spectrometer. The spectra were obtained in a Bruker micrOTOF operating in positive ESI+ mode, 1.0 μL loop injection, 50:50 methanol:water solvent flowing at 10 μL/min (for other details, see the Supporting Information). On some occasions, the product mixture was injected to the mass spectrometer thru an Eksigent nanoLC 2D system using an Ace 300 Å C18 HPLC column (0.5 mm × 150 mm, 3 μm particle size). All details are provided in the Supporting Information.

2.2. Analytical Ultracentrifugation Analysis (AUC).

Samples at various stages of purification (Table S1 and Figure S1) were analyzed using a Beckman Optima AUC analytical ultracentrifuge operating at two speeds (30,000 and 40,000 rpm) and two wavelengths (240 and 330 nm). Sedimentation coefficient distributions for various purification steps are summarized in Figures S2–S4 (diffusion corrected s-value distribution).

2.3. Susceptibility Testing Assays for the Examination of Activity Against Planktonic Bacteria and Fungal Biofilms.

Antifungal activity was evaluated on *Candida albicans* wild-type strain SC5314 on preformed biofilms of *C. Albicans* by well-established phenotypic assays as detailed in the SI section. The IC_{50} was calculated from the dose–response nonlinear curves using a weighted nonlinear curve fitting determined by fitting the data using the software Origin 9. Anti-MRSA minimal inhibitory concentration (MIC) of $Ag_{29}(LA)_{12}$ was obtained by broth microdilution methods as detailed in the Supporting Information. All experiments were performed in duplicate and repeated a minimum of three times.

2.4. Theoretical Calculations (DFT).

First-principle quantum-chemical calculations were performed starting with the experimental coordinates published for the nonaqueous homologue of the $Ag_{29}(LA)_{12}$ cluster.[21] The spin-polarized density-functional theory (DFT) calculations were performed with the SIESTA code,[26] and then VASP, as detailed in the Supporting Information.

3.0. RESULTS AND DISCUSSION

3.1. Composition via Electrospray Ionization Mass Spectrometry (ESI-MS).

Aqueous samples of the cluster are prepared by a modification of prior methods,[19] according to the steps in Scheme 1, but gave optical spectra (absorbance, luminescence, circular dichroism) that match the published reports.[18] Under gentle ionization conditions and

judicious ion-pairing pretreatment, the 29-atom cluster maybe detected intact (Figure 1A). Specifically, treatment of the pendant acidic groups with the volatile base triethylamine (TEA), yields the ion-paired forms with triethylammonium ($TEAH^+$), and suppresses the formation of sodium adducts and the concomitant propensity of the sodiated cluster to salt out of solution during ESI-MS analysis.[19] As detailed separately, alkali adducts may be removed by first precipitating the cluster with dilute acetic acid and then redissolving it in an aqueous solution containing excess TEA.[27]

Further analysis[28] by inline capillary HPLC-UV-ESI-MS confirms that this aqueous 5,6-kDa species can be easily separated from low-mass reaction byproducts, as well as any higher species, prior to the ESI-MS detection, reducing the likelihood that it is a product of gas-phase aggregation or degradation. Under optimized conditions, HPLC resolves two components, of essentially equal abundance, showing identical optical absorption and ESI mass-spectra. It has been suggested that this is consistent with a pair of diastereomers (cf. structure analysis below).[28]

Gas-phase cluster fragmentation may be induced in the ion transmission section, prior to the mass spectrometer. Increasing the voltage between capillary exit and collimating skimmer increases the momentum with which the cluster collides with the background gas as it translates from a higher-pressure source region to a lower pressure. Inducing collisional fragmentation in this manner results first in the ejection of one ligand, then another from the cluster while conserving the number of silver atoms intact at 29 (Figure 1B).

As reported previously, the polyanionic form is highly prone to fragmentation, and under collisional dissociation conditions the cluster can fragment to yield silver-lipoate oligomers.[19]

3.2. Electronic Shell Structure Inferred from ESI-MS Results and SAC Model.

The observation of the intact cluster is significant because it establishes the compositional assignment to 29 silver atoms and 12 ligands while attesting to its structural stability or resilience. Also notable are the numbers of $TEAH^+$ cations adducted to the cluster at various charge states: The Figure 1A labels show that the singly charged cluster ($z = 1+$) is adducted by four (4) TEAH+ cations, which provides direct evidence that the adduct-free cluster holds a [3-]-charge state, as had been suspected previously.[19] Similarly, the major feature in Figure 1A, labeled $[(29,12) + 5\ TEAH]^{2+}$, may be rewritten as $[(29,12)^{3-} + 5\ TEAH^+]$, in the standard notation.

In turn, the charge-state [3−] suggests that the cluster is stabilized by a “magic” number of free electrons (n) of eight (8), as predicted by the Super-Atom Complex (SAC) model[29] and anticipated by others,[19] i.e., $[(Ag)_{29}(RS_2)_{12}]^{3-} = (Ag^+)_{29}(RS_2{}^{2-})_{12}(e^-)_8$. More formally, this model predicts the number of free (unassociated) electrons, n, of a species $(A_nX_m)^z$ of net charge z from the number N of metal atoms of valence v_A and the number M of ligands X of valence v_X.

$$n = v_A N - v_X M - z \tag{1}$$

A cluster is predicted to be stable when $n = n^*$, a ("magic") number associated with shell closings (n^* = 2, 8, 18, 34, 58, 92, 128, 198, 274, 368, …). Indeed, for the $[Ag2_9(LA)_{12}]^{3-}$ complex, eq 1 yields $n^* = 8$, from the parameter set $\{N = 29, v_A = 1, M = 12, v_X = 2, z = -3\}$.

The $[Ag_{29}(LA)_{10}]^+$ signal that dominates the fragmentation spectra (Figure 1B) also has an electron count of $n^* = 8$, i.e., 29 − (2)10 − 1, consistent with an overall charge-state of $z = 1+$, which explains why it is observed abundantly without TEAH+ adducts. Less dominant fragment ions in Figure 1B are predicted to have open shells, as may be verified by substituting their composition in eq 1.

The nonaqueous counterpart exhibits an icosahedral-tetrahedral structure as demonstrated by Bakr and collaborators.[21] However, to obtain direct structural information on the aqueous cluster described here from electron microscopy or X-ray diffraction measurements at the present stage of this investigation. As a result, we rely on the experimentally determined structure for the nonaqueous counterpart as a starting point for theoretical modeling and interpretation of mass spectrometry results. Specifically, we assume that the aqueous cluster exhibits an icosahedral-tetrahedral structure, as determined by Abdul-Halim et al.,[21] and is "tetravalent", i.e., it is most stable when coordinated with four (4) weakly bound ligands, PPh_3, identified in the crystal structure as well as in ESI-MS detection. It also has three (3) counter-cations, which were not identified.[21]

3.3. First-Principles (DFT) Analysis of Structure Models.

In order to gain further insight we have performed first-principles quantum-chemical calculations on models derived from the coordinate-set of the crystallographic structure.[21] Our strategy was first to replace phenyl groups by hydrogen atoms (PH_3 in place of PPh_3), and let it relax to its optimal structure. From this structure, a second, minimal model was obtained by replacing each of the 12 dithiolate ligands by a pair of chloride (Cl^-) ions, i.e., iso-electronic substitution, one Cl-atom taking the site of each S atom, prior to reoptimization.[30]

In every case, the [3−] charge-state was assumed, and an essentially similar structure was obtained (Figure 2). The optimized structures each show a set of triply degenerate HOMOs, and a substantial HOMO–LUMO gap, approaching 2.0 eV, consistent with the optical absorption spectra, which show an onset of strong absorption in this (red) region. We believe these are sufficient to explain the special stability of the $(29,12)^{[3-]}$ complex, although we have not yet attempted to construct models with the probable configurations of the methylene units separating the pairs of sulfur head-groups, as was initiated previously in the work by Russier-Antoine et al.[20]

3.4. Chirality (HCM) Analysis.

Other interesting facts arising from the theoretical analysis of these models concern the exact chiral-tetrahedral symmetry (*T*-group) of the optimized complex, and the very large magnitude of the Hausdorff chirality measure (HCM),[31] the latter being consistent with the recent observations[18] of a strong CD spectrum (also confirmed in our work) and the remarkable phenomenon of red circularly polarized luminescence. Figure 3 shows the

decomposition of these two model structures into core (Ag_{13}) and shell ($Ag_{16}X_{24}$) assemblies, and further indicates how sets of symmetry-equivalent atoms, or groups, are used to calculate the HCM values.[32]

The core (Ag_{13}) has a low HCM value (~0.02), consistent with its usual description as icosahedral, when in fact it exhibits clearly the symmetry lowering from I_h- to *T*-symmetry. The shell has a large HCM value, indicative of intrinsic chirality, in the T-symmetry group, and suggesting high optical activity: HCM ≈ 0.14 in the case of the X = Cl model, and HCM ≈ 0.16 for the benzene-dithiolate structure that was determined by single-crystal X-ray diffraction methods. These values are near the high end of those catalogued in a recent study on quantification of chirality in protected noble-metal clusters.[32]

The compositional (and charge) certainty provided by our new experiments, augmented by the theoretical analysis of realistic structure models, should also provide a basis for understanding the spectroscopic and other phenomena already reported.[18–20]

3.5. Hydrodynamic Size Characterization via AUC analysis.

Solution-phase analytical ultracentrifugation (AUC) further provides a comprehensive and quantitative measure of its purification as presented in Figure S1. Sedimentation distributions revealed one major species present at each stage of purification with a sedimentation coefficient of 4.21 s and a diffusion coefficient of 14.48×10^{-7} cm^2/s, corresponding to a Stokes radius of ~1.49 nm (diameter ~3.0 nm) as summarized in Figure 4.

In addition, several minor peaks were visible which changed in relative concentration and position as a function of purification step (Figure S1). The relatively small cluster size and the tendency of the cluster to form ions are expected to play important roles in the antibiotic action of the cluster.

3.6. Activity Against Planktonic Bacterial Cultures and Fungal Biofilms.

Prior research has established that silver nanoparticles (AgNPs) exhibit bactericidal effects against *Staphylococcus aureus* bacteria, including the methicillin-resistant *Staphylococcus aureus* (MRSA),[1,9,33–35] as well as antifungal effects against planktonic *Candida albicans*,[36,37] and against *Candida* biofilms.[38–40] Thus, $Ag_{29}LA_{12}$ was tested using in vitro susceptibility methods[35] against a MRSA strain (MIC) and against preformed biofilms of C. *albicans* (IC_{50}) as detailed in the Supporting Information. Fluorescence-based assays[35] could not be used to assess the phenotypic assays because of the interference from the native fluorescence emanating from the clusters.[17–21] To the best of our knowledge, this is the first time that this cluster has been tested for its antibacterial or antifungal properties.

C. *albicans* biofilms were inhibited by $Ag_{29}LA_{12}$ in a dose–response manner, with a half maximal inhibitory concentration[35] (IC_{50}) of 0.94 mg of Ag/mL (Figure 5). A separate control test was performed using neat LA to ensure that the antifungal effect was NOT caused by the presence of excess LA in the raw cluster product. It is estimated from the actual stoichiometric ratios employed in the synthesis that the raw cluster product has a silver concentration of 1.2 mg of Ag/mL and a LA concentration of 13 mg of LA/mL.

Therefore, the IC_{50} dose of 0.94 mg of Ag/mL corresponds to a LA concentration of 10 mg-LA/mL. Neat LA was found to be inhibitory at concentrations of 31.7 mg of LA/mL and 15.7 mg of LA/mL but NOT at 8 mg of LA/mL or below. It can therefore be concluded that the inhibitory effect of the cluster at 0.94 mg-Ag/mL is NOT due to LA alone. However, the role of alkaline conditions in the inhibitory action of neat LA at high concentrations >15.7 mg of LA/mL cannot be ruled out because addition of a base is needed to raise the pH of the control solution to 8–10 units to dissolve lipoic acid at those concentrations. Comparing these results to previous research with AgNPs (IC_{50} 0.4–3.2 μg/mL)[12,38] we needed much higher concentrations of $Ag_{29}LA_{12}$ to achieve comparable inhibitory effects against these fungal biofilms.

To test the bactericidal activity against MRSA strain TCH1516, we determined the minimal inhibitory concentrations[35] (MICs) using broth microdilution methods as described in the Supporting Information.

The corresponding minimum inhibitory concentration (MIC) determined by these assays was 0.6 mg of Ag/mL. A control test on MRSA revealed that neat LA inhibited MRSA only at concentrations of 31.7 mg of LA/mL. Therefore, LA alone is NOT responsible for the antibiotic activity of the cluster solution on MRSA Comparing our results with previous results with those reported previously for pure AgNPs (MIC 0.2–100 μg/mL),[13,41–43] much higher concentrations of $Ag_{29}LA_{12}$ are required to achieve comparable inhibitory effects against MRSA.

In one study characterizing the bactericidal activity of 10 nm silver particles stabilized with lipoic acid, Niska et al.[41] report MIC values in the 5–40 μg/mL range on all Gram-positive bacteria tested, including MRSA. Above 40 μg/mL, the LA-capped particles were toxic to human gingival fibroblast cells (HGF-l). Silver nitrate, used as a reference in their study, inhibited at 5–100 μg/mL concentrations, was toxic at 5 μg/mL, but was not effective on all bacteria tested.[41]

3.7. Electron Microscopy to Assess the Effects of the Clusters on Microbial Cells.

Elucidating the mechanism of action of these clusters is beyond the scope of the present report but the mechanism of AgNPs has been studied extensively by others.[44,45] However, we used Advanced Electron Microscopy (AEM) techniques in order to provide some initial insights into the effects of our clusters on bacterial and fungal cells. SEM images (Figure 6) of preformed biofilm of *Candida albicans*, pretreatment display true hyphae and yeast cells display a smooth surface on the cell wall (CW) and a dense mesh-like network of yeasts cells and hyphal elements. After 24 h treatment of clusters, at 0.94 mg-Ag/mL, the preformed biofilm of *Candida albicans* shows scarce hyphae, disrupted outer cell walls, and the silver has become aggregated. Contrasting SEM images of MRSA cells, without treatment vs post-treatment, show cell size and morphology changes of MRSA along with clusters interacting and agglomerated on the outer cell surface. Cluster concentration was 0.6 mg of Ag/mL for 24 h of treatment.

Previously, for larger particles, Morones et al.[9] demonstrated that positively charged silver nanoparticles bind to the negatively charged outer cell wall of MRSA bacteria resulting in

membrane permeability, and bacterial lysis as shown in Figure 6d by advanced electron microscopy (AEM) detailed in the Supporting Information, and generation of reactive oxygen species (ROS), with release of silver cations.[9] Similarly, previous research demonstrated that the fungicidal action of AgNPs against C. *albicans* is due to the disruption of the outer cell membrane/wall, inhibition of filamentation, permeabilization of the cell wall, and disruption of the structural layers of the outer fungal cell wall as shown in Figure 6b.[37,38]

Regarding smaller particles or clusters, by using advanced electronic microscopy (AEM) techniques, others have shown that silver nanoclusters aggregate inside the cell after permeabilization.[33,36,38]

Silver nanoclusters, as investigated herein, may be regarded as very small nanoparticles. Previous in vitro results demonstrated that smaller size in AgNPs enhance bactericidal efficacy and lessen cytotoxicity.[42,46] In vivo studies reported that use of smaller silver nanoparticles (diameter <6 nm) enhance the renal clearance with a rapid and efficient urinary excretion.[15,16] A key advantage of clusters is that they can easily be eliminated by the kidney in animal models and humans.[47]

One possible reason for the apparent high MIC values exhibited by the Ag_{29} cluster could be its exceptional aqueous-phase stability relative to other silver particle systems. Most mechanisms for the bactericidal activity of silver particles propose the generation of silver cations as an intermediate.[10–14]

In aqueous cellular environment, nanoparticles are hypothesized to fall apart and release silver cations that inhibit cellular transport proteins. If the $Ag_{29}LA_{12}$ cluster, contrary to the more reactive larger particles, remains intact for a longer period, that would explain the higher MIC numbers observed during the 24 h incubation tests. It is possible that the cluster exhibits longer term action, a feature that may prove beneficial and at least guarantees further studies and alternative antibiotic assays. In addition, the higher MIC values observed for the cluster may also be due to its [–3] charge state that, when dissociated in an aqueous environment, may result in a charge barrier that must be surpassed to allow the negatively charged cluster anion to interact with membrane walls (also presumed to be negatively charged). Such barriers have not hindered the antibiotic activity of larger negatively charged particles.[48] The $Ag_{29}LA_{12}$ cluster, as demonstrated during mild ES-MS measurements (Figure 1), easily forms intact cations at physiological pH. Proper pH control may thus be needed to increase the antibiotic activity of the cluster.

We are fully aware that the minimum inhibitory concentrations reported here from phenotypic assays for the $Ag_{29}LA_{12}$ cluster are too high to be applied systemically, as one expects these high concentrations to be cytotoxic.[12,49,50] However, the cluster could potentially be used in different treatment modalities, such as topical applications (i.e., wound infections, disinfection) and, in the case of biofilms, in catheter lock therapy in which high suprapharmacological concentrations of antimicrobial agents are instilled into the lumen of infected catheters to try to overcome the intrinsic resistance of cells within the biofilms.[3,51,52]

4. CONCLUDING REMARKS

In addition to exhibiting unique electronic properties arising from its 8-electron shell closing, the $Ag_{29}LA_{12}$ cluster exhibits antibacterial properties against antibiotic resistant MRSA and anti-fungal activity against C. *albicans* preformed biofilms. Although higher concentrations of the cluster are needed for inhibitory activity than those reported for larger silver nanoparticles, the $Ag_{29}LA_{12}$ cluster offers the likely benefits of the ligand being biocompatible and biodegradable, not to mention greatly enhanced stability ("shelf life") and the assurance of a certified chemical composition and purity.

In conclusion, the novel contributions of this work include the following:

1. For the first time, we have established the bactericidal and fungicidal activity of a unique silver cluster of well-known composition and electronic structure.
2. Twelve biocompatible lipoate ligands per cluster offer myriad possibilities for bioconjugation of the carboxylic group with antibiotic compounds, such as penicillin, to enhance the cluster effectiveness.
3. In addition, the surface ligands may be conjugated with various anchoring agents and chromophores for targeting specific cell components (lipid bilayer and membrane proteins)
4. The electronic structure and composition of the aqueous cluster has been elucidated
5. The cluster exhibits an extraordinary chirality, as first quantified herein.

Continuing work involves the bioconjugation of the silver lipoate clusters to antibiotics, such as ampicillin and penicillin G, and the exploration of alternative assays to probe the long-term activity of the cluster. In addition, we continue to study the nature of the four elusive coordinating ligands and three counterions and how these affect the stability of this intriguing magic-sized cluster.

Supplementary Material

Refer to Web version on PubMed Central for supplementary material.

ACKNOWLEDGMENTS

This work has been supported by The Welch Foundation Grant AX-1615 (M.J.Y.) and Grant AX-1857 (R.L.W.). Additional support was provided by the Margaret Batts Tobin Foundation, San Antonio, TX (J.L.L.-R.). Sedimentation velocity experiments were analyzed with UltraScan using the XSEDE UltraScan Science Gateway supported by NSF grants ACI-1339649 and TG-MCB070039 and NIH grant R01GM120600 (all three to B.D.). HCM calculations were performed at the DGTIC-UNAM Supercomputing Center. This work has used HPC resources from GENCI-IDRIS (Grant 2017–096829). ILG thanks support from DGAPA-UNAM under Project IN108817 and Conacyt-Mexico under Project 285821 Authors acknowledge valuable contributions from Professor Lorenzo Brancaleon, Dr. Ekaterina Vinogradova, Dr. Josefina Arrellano-Jimenez, Mr. Geronimo Robles, Mr. Aaron Mendlowitz, and Mr. Jon Staggs.

REFERENCES

(1). Ayala-Núñez NV; Lara-Villegas HH; del Carmen Ixtepan-Turrent L; Rodríguez-Padilla C Silver Nanoparticles Toxicity and Bactericidal Effect Against Methicillin-Resistant Staphylococcus aureus: Nanoscale Does Matter. NanoBiotechnology 2009, 5, 2–9.

(2). Lara HH; Garza-Treviño EN; Ixtepan-Turrent L. d. C.; Singh DK Silver Nanoparticles are Broad-spectrum Bactericidal and Virucidal Compounds. J. Nanobiotechnol 2011, 9, 30.

(3). Rai M; Yadav A; Gade A Silver Nanoparticles as a New Generation of Antimicrobials. Biotechnol. Adv 2009, 27, 76–83. [PubMed: 18854209]

(4). Antibiotic/Antimicrobial Resistance; Centers for Disease Control and Prevention: Atlanta, 2017.

(5). McShan D; Zhang Y; Deng H; Ray PC; Yu H Synergistic Antibacterial Effect of Silver Nanoparticles Combined with Ineffective Antibiotics on Drug Resistant Salmonella Typhimurium DT104. J. Environ. Sei. Health C 2015, 33, 369–384.

(6). Lara HH; Ayala-Núnez NV; Ixtepan-Turrent L d. C.; Rodriguez Padilla, C. Bactericidal Effect of Silver Nanoparticles Against Multidrug-Resistant Bacteria. World J. Microbiol. Biotechnol 2010, 26, 615–621.

(7). Lok CNHo CM; Chen R; He QY; Yu WY; Sun H; Tam P. k.; Chiu JF; Che CM Proteomic Analysis of the Mode of Antibacterial Action of Silver Nanoparticles. J. Proteome Res. 2006, 5, 916–24. [PubMed: 16602699]

(8). Foster TJ Antibiotic Resistance in Staphylococcus Aureus. Current Status and Future Prospects. FEMS Microbiol Rev. 2017, 41, 430–449. [PubMed: 28419231]

(9). Morones JR; Elechiguerra JL; Camacho A; Holt K; Kouri JB; Ramirez JT; Yacamán MJ The Bactericidal Effect of Silver Nanoparticles. Nanotechnology 2005, 16, 2346–53. [PubMed: 20818017]

(10). Morones-Ramirez JR; Winkler JA; Spina CS; Collins JJ Silver Enhances Antibiotic Activity Against Gram-negative Bacteria. Sci. Transl. Med 2013, 5, 190ra81.

(11). Durán N; Duran M; Bispo de Jesus M; Seabra AB; Fávaro WJ; Nakazato G Silver Nanoparticles: A New View on Mechanistic Aspects on Antimicrobial Activity. Nanomedicine 2016, 12, 789–99. [PubMed: 26724539]

(12). Naik K; Kowshik M The silver lining: Towards the Responsible and Limited Usage of Silver. J. Appl. Microbiol 2017, 123, 1068–1087. [PubMed: 28650591]

(13). Franci G; Falanga A; Galdiero S; Palomba L; Rai M; Morelli G; Galdiero M Silver Nanoparticles as Potential Antibacterial Agents. Molecules 2015, 20, 8856–74. [PubMed: 25993417]

(14). Natan M; Banin E From Nano to Micro: Using Nanotechnology to Combat Microorganisms and their Multidrug Resistance. FEMS Microbiol. Rev 2017, 41, 302–22. [PubMed: 28419240]

(15). Soo Choi H; Liu W; Misra P; Tanaka E; Zimmer JP; Itty Ipe B; Bawendi MG; Frangioni JV Renal Clearance of Nanoparticles. Nat. Biotechnol 2007, 25, 1165–1170. [PubMed: 17891134]

(16). Longmire M; Choyke PL; Kobayashi H Clearance Properties of Nano-sized Particles and Molecules as Imaging Agents: Considerations and Caveats. Nanomedicine 2008, 3, 703–717. [PubMed: 18817471]

(17). Baksi A; Ghosh A; Mudedla S. k.; Chakraborty P; Bhat S; Mondai B; Krishnadas KR; Subramanian V; Pradeep T Isomerism in Monolayer Protected Silver Cluster Ions: An Ion Mobility-Mass Spectrometry Approach. J. Phys. Chem. C 2017, 121, 13421–27.

(18). Kumar J; Kawai T; Nakashima T Circularly Polarized Luminescence in Chiral Silver Nanoclusters. Chem. Commun 2017, 53, 1269–72.

(19). van der Linden M; Barendregt A; van Bunningen AJ; Chin PT; Thies-Weesie D; de Groot FM; Meijerink A Characterisation, Degradation and Regeneration of Luminescent Ag 29 Clusters in Solution. Nanoscale 2016, 8, 19901–9. [PubMed: 27878182]

(20). Russier-Antoine I; Bertorelle F; Hamouda R; Rayane D; Dugourd P; Sanader Ž; Bonačić-Koutecký V; Brevet PF; Antoine R Tuning Ag29 Nanocluster Light Emission from Red to Blue with One and Two-photon Excitation. Nanoscale 2016, 8, 2892–8. [PubMed: 26765164]

(21). AbdulHalim LG; Bootharaju MS; Tang Q; Del Gobbo S; AbdulHalim RG; Eddaoudi M; Jiang DE; Bakr OM Ag29 (BDT) 12 (TPP) 4: A Tetravalent Nanocluster. J. Am. Chem. Soc 2015, 137, 11970–5. [PubMed: 26104755]

(22). Shay KP; Moreau RF; Smith EJ; Smith AR; Hagen TM Alpha-lipoic Acid as a Dietary Supplement: Molecular Mechanisms and Therapeutic Potential. Biochim. Biophys. Acta, Gen. Subj 2009, 1790, 1149–60.

(23). Kwiecień B; Dudek M; Bilska-Wilkosz A; Knutelska J; Bednarski M; Kwiecień I; Zygmunt M; Iciek M; Sokolowska-Jezewicz M; Sapa J; Wlodek L In Vivo Anti-inflammatory Activity of Lipoic Acid Derivatives in Mice. J. Sapa, Postepy. Hig. Med. Dosw 2013, 67, 331–338.

(24). Patel MS; Lester P, Eds. Lipoic Acid Energy Production In Antioxidant Activity and Health Effects; CRC Press: Boca Raton, FL, 2008.

(25). Gruzman A; Hidmi A; Katzhendler J; Haj-Yehie A; Sasson S Synthesis and Characterization of New and Potent α-Lipoic Acid Derivatives. Bioorg. Med. Chem 2004, 12, 1183–90. [PubMed: 14980629]

(26). Soler JM; Beltran MR; Michaelian K; Garzón IL; Ordejón P; Sánchez-Portal D; Artacho E Metallic bonding and cluster structure. Phys. Rev. B: Condens. Matter Mater. Phys 2000, 61, 5771–5780.

(27). Black DM; Alvarez MM; Yan F; Griffith WP; Plascencia-Villa G; Bach SB; Whetten RL Triethylamine Solution for the Intractability of Aqueous Gold–Thiolate Cluster Anions: How Ion Pairing Enhances ESI-MS and HPLC of aq-Aun(pMBA)p. J. Phys. Chem. C 2017, 121, 10851–7.

(28). Black DM; Robles G; Lopez P; Bach SBH; Alvarez M; Whetten RL Liquid Chromatography Separation and Mass Spectrometry Detection of Silver-Lipoate Ag29(LA)12 Nanoclusters: Evidence of Isomerism in the Solution Phase. Anal. Chem 2018, 90, 2010–2017. [PubMed: 29260853]

(29). Walter M; Akola J; Lopez-Acevedo O; Jadzinsky PD; Calero G; Ackerson CJ; Whetten RL; Grönbeck H; Häkkinen H A Unified View of Ligand-protected Gold Clusters as Superatom Complexes. Proc. Natl. Acad. Sci. U. S. A 2008, 105, 9157–62. [PubMed: 18599443]

(30). Jiang D-E; Walter M The Halogen Analogs of Thiolated Gold Nanoclusters. Nanoscale 2012, 4, 4234–4239. [PubMed: 22539033]

(31). Buda AB; Mislow K A Hausdorff Chirality Measure. J. Am. Chem. Soc 1992, 114, 6006–6012.

(32). Pelayo JJ; Whetten RL; Garzón IL Geometric Quantification of Chirality in Ligand-Protected Metal Clusters. J. Phys. Chem. C 2015, 119, 28666–28678.

(33). Romero-Urbina DG; Lara HH; Velázquez-Salazar JJ; Arellano-Jiménez MJ; Larios E; Srinivasan A; Lopez-Ribot JL; Yacamán MJ Ultrastructural Changes in Methicillin-Resistant Staphylococcus Aureus Induced by Positively Charged Silver Nanoparticles. Beilstein J. Nanotechnol 2015, 6, 2396–405. [PubMed: 26734530]

(34). Ansari MA; Khan HM; Khan AA; Cameotra SS; Alzohairy MA Anti-Biofilm Efficacy of Silver Nanoparticles Against MRSA and MRSE Isolated from Wounds in a Tertiary Care Hospital. Indian J. Med. Microbiol 2015, 33, 101–9. [PubMed: 25560011]

(35). Karaman DŞ; Manner S; Fallarero A; Rosenholm JM Current Approaches for Exploration of Nanoparticles as Antibacterial Agents. In Antibacterial Agentsj InTech Open: Reijeka, Croatia, 2017; Chapter 4.

(36). Vazquez-Muñoz R; Avalos-Borja M; Castro-Longoria E Ultrastructural Analysis of Candida albicans when Exposed to Silver Nanoparticles. PLoS One 2014, 9, e 108876.

(37). Kim KJ; Sung WS; Suh B. k.; Moon S. k.; Choi JS; Kim JG; Lee DG Antifungal Activity and Mode of Action of Silver Nano-Particles on Candida albicans. BioMetals 2009, 22, 235–42. [PubMed: 18769871]

(38). Lara HH; Romero-Urbina DG; Pierce C; Lopez-Ribot JL; Arellano-Jimenéz MJ; José-Yacamán M Effect of Silver Nanoparticles on Candida albicans Biofilms: An Ultrastructural Study. J. Nanobiotechnol 2015, 13, 91.

(39). Monteiro DR Silver Colloidal Nanoparticle Stability: Influence on Candida Biofilms Formed on Denture Acrylic. Med. Mycol 2014, 52, 627–635. [PubMed: 24951722]

(40). Monteiro DR; Silva S; Negri M; Gorup LF; de Camargo ER; Oliveira R; Barbosa DDB; Henriques M Silver Colloidal Nanoparticles: Effect on Matrix Composition and Structure of

Candida albicans and Candida glabrata Biofilms. J. Appl. Microbiol 2013, 114, 1175–1183. [PubMed: 23231706]

(41). Niska k.; Knap N; Kędzia A; Jaskiewicz M; Kamysz W; Inkielewicz-Stepniak I Capping Agent-dependent Toxicity and Antimicrobial Activity of Silver Nanoparticles: An In vitro Study. Concerns About Potential Application in Dental Practice. Int. J. Med. Sei 2016, 13, 772–82.

(42). Paredes D; Ortiz C; Torres R Synthesis, Characterization, and Evaluation of Antibacterial Effect of Ag Nanoparticles Against Escherichia coli O157: H7 and Methicillin-Resistant Staphylococcus aureus (MRSA). Int. J. Nanomed 2014, 9, 1717–1729.

(43). Sheikholeslami S; Mousavi SE; Ahmadi Ashtiani HR; Hosseini Doust SR; Mahdi Rezayat S Antibacterial Activity of Silver Nanoparticles and Their Combination with Zataria multiflora Essential Oil and Methanol Extract. Jundishapur J. Microbiol 2016, 9, e36070. [PubMed: 27942360]

(44). Zheng K; Setyawati MI; Leong DT; Xie J Antimicrobial Silver Nanomaterials. Coord. Chem. Rev 2018, 357, 1–17.

(45). Wu WY; Yang Y; Zhang Z; Wang Z; Zhao Y; Sun LA Facile Method to Prepare Size-tunable Silver Nanoparticles and its Antibacterial Mechanism. Adv. Powder Technol 2018, 29, 407–415.

(46). Lu Z; Rong k.; Li J; Chen Y Size-dependent Antibacterial Activities of Silver Nanoparticles Against Oral Anaerobic Pathogenic Bacteria. J. Mater. Sei.: Mater. Med. 2013, 24, 1465–1471.

(47). Hoshyar N; Gray S; Han HB; Bao G The Effect of Nanoparticle Size on In Vivo Pharmacokinetics and Cellular Interaction. Nanomedicine 2016, 11, 673–692. [PubMed: 27003448]

(48). Salvioni L; Galbiati E; Collico V; Alessio G; Avvakumova S; Corsi F; Tortora P; Prosperi D; Colombo M Negatively Charged Silver Nanoparticles with Potent Antibacterial Activity and Reduced Toxicity for Pharmaceutical Preparations. Int. J. Nanomed 2017, 12, 2517.

(49). Calderón-Jiménez B; Johnson ME; Montoro Bustos AR; Murphy KE; Winchester MR; Vega Baudrit JR Silver Nanoparticles: Technological Advances, Societal Impacts, and Metro-logical Challenges. Front. Chem 2017, 5, 6. [PubMed: 28271059]

(50). Foldbjerg R; Jiang X; Miclăuş T; Chen C; Autrup H; Beer C Silver Nanoparticles—Wolves in Sheep's Clothing? Toxicol. Res 2015,4, 563–75.

(51). Cao H, Ed. Silver Nanoparticles for Antibacterial Devices: Bio compatibility and Toxicity, CRC Press: Boca Raton, FL, 2017.

(52). Justo JA; Bookstaver PB Antibiotic Lock Therapy: Review of Technique and Logistical Challenges. Infect. Drug Resist 2014, 7, 343–63. [PubMed: 25548523]

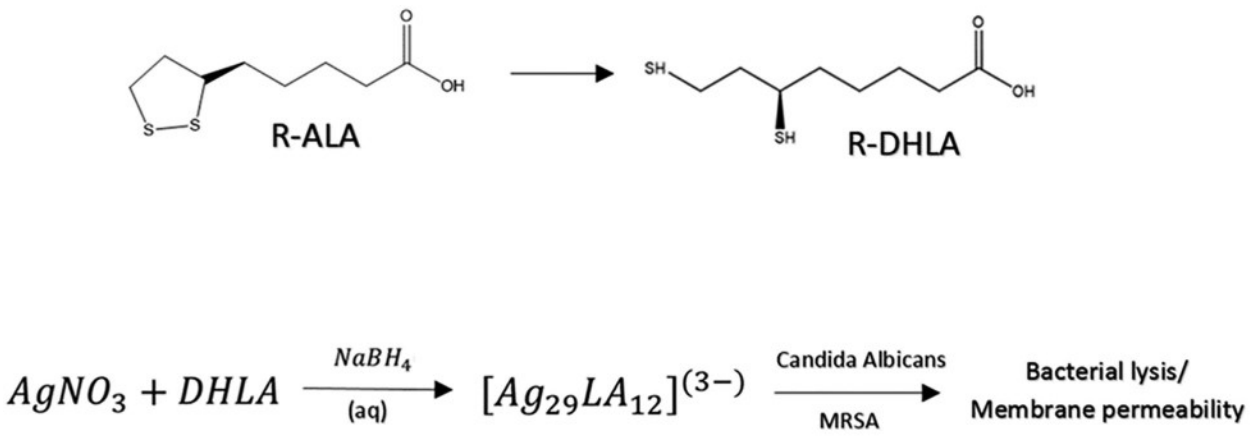

Scheme 1. Process of R-α-Lipoic Acid Reduction to R-Dihydrolipoic Acid, Then Added to Silver Nitrite and Excess Sodium Borohydride to Produce the Cluster-Complex $Ag_{29}LA_{12}$[a]

[a]All reagents are in the aqueous phase.

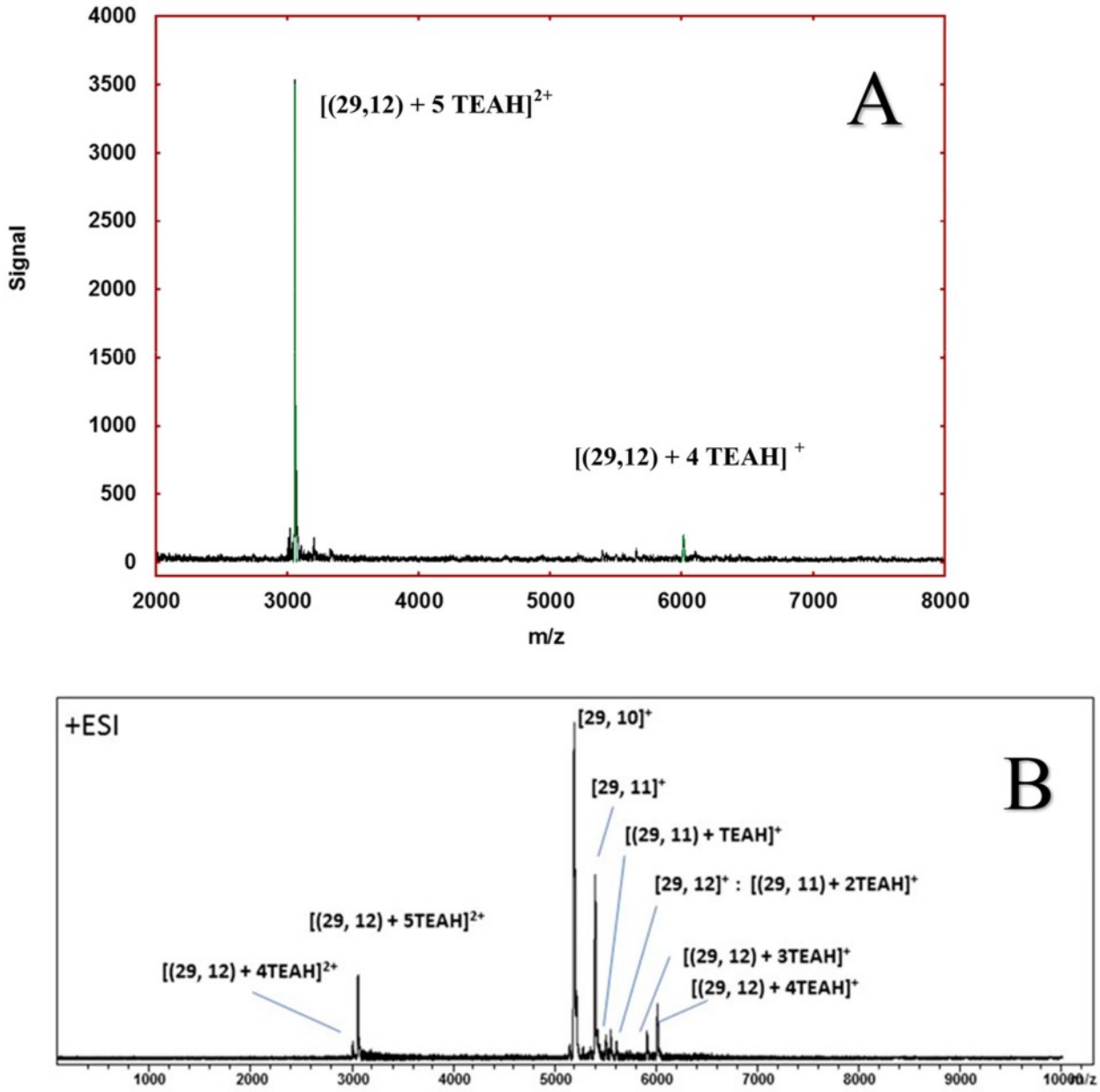

Figure 1.

Electrospray ionization mass spectrometric analysis of the Ag_{29} lipoate complex in solution. (A) Cluster can be detected intact thus confirming its composition and 3- charge state. The observed peak positions and isotopic patterns agree with those calculated (green trace) from the chemical formulas given, assuming all lipoic acid carboxyl groups are protonated ($-CO_2H$). (B) Cluster can be induced to fragment by loss of lipoate ligands while keeping its silver count intact at 29.

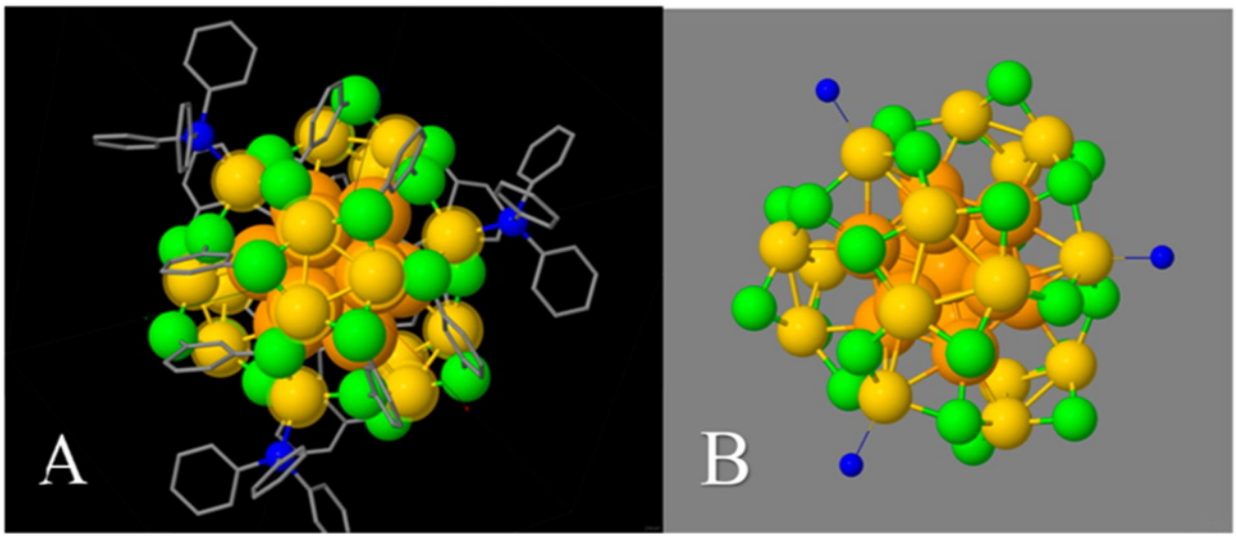

Figure 2.

Structure models optimized by DFT calculations show how (B) an isoelectronic aqueous surrogate of the $(29,12)^{(3-)}$ cluster retains (A) the structural features of its nonaqueous homologue. Viewed along a C_3-axis. Color code: Ag (orange, gold, yellow spheres); S or Cl (lime-green); P (blue); C (gray); H (not shown). See text for details of these models.

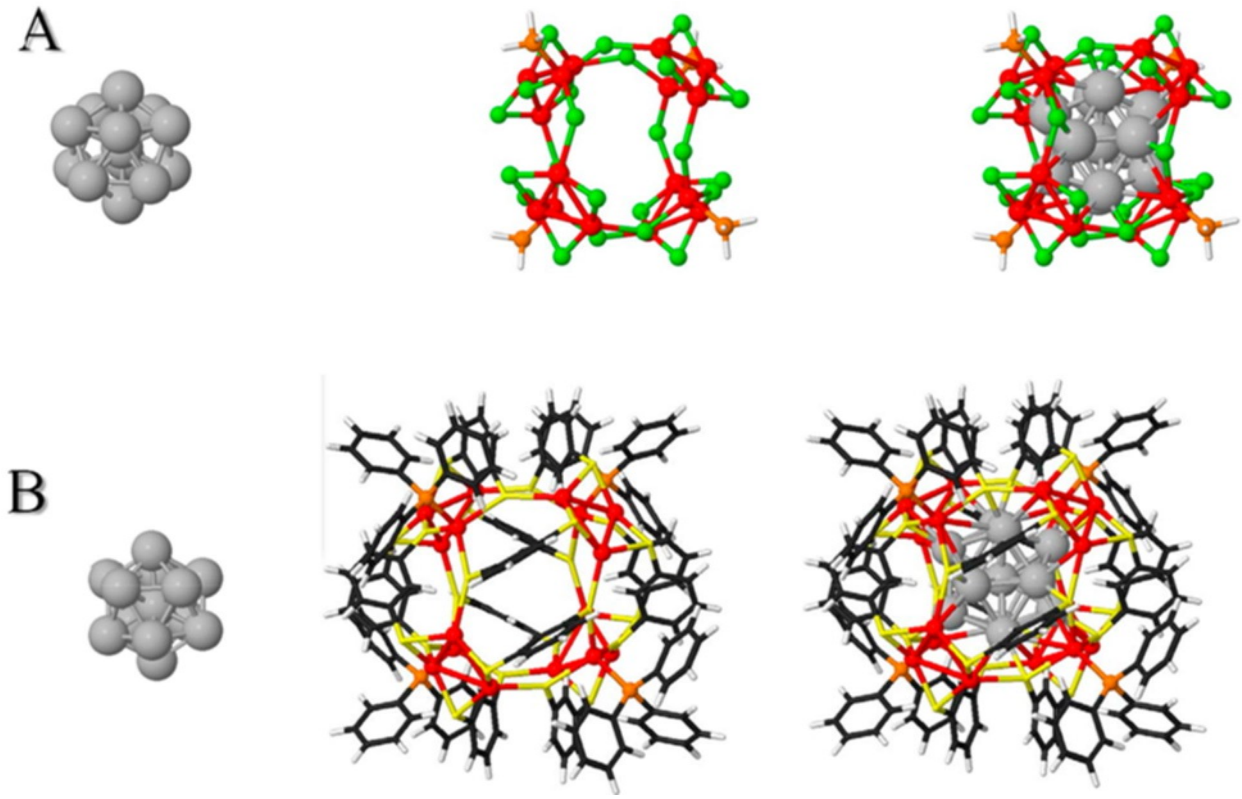

Figure 3.

Core (left), shell (center), and core+shell (right) model structures (cf. Figure 2) used for the calculation of the HCM index of chirality : (A) $Ag_{29}Cl_{24}(PH_3)_4$ and (B) $Ag_{29}(S_2Ph)_{12}(PPh_3)_4$. Color code: Ag (gray or red spheres); S (yellow) or Cl (lime-green); P (orange); C (black); H (white).

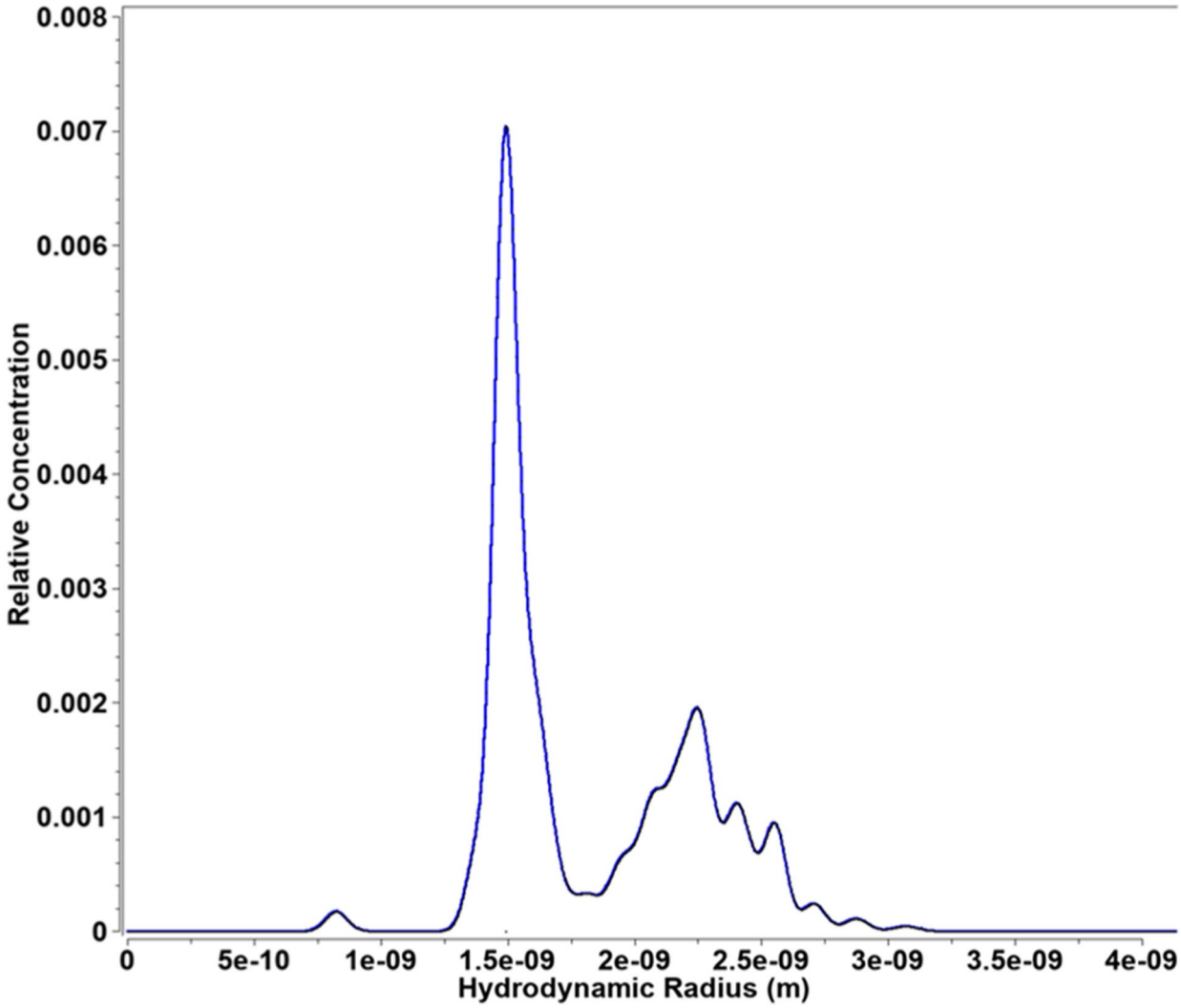

Figure 4.
Stokes radius distribution after cluster purification.

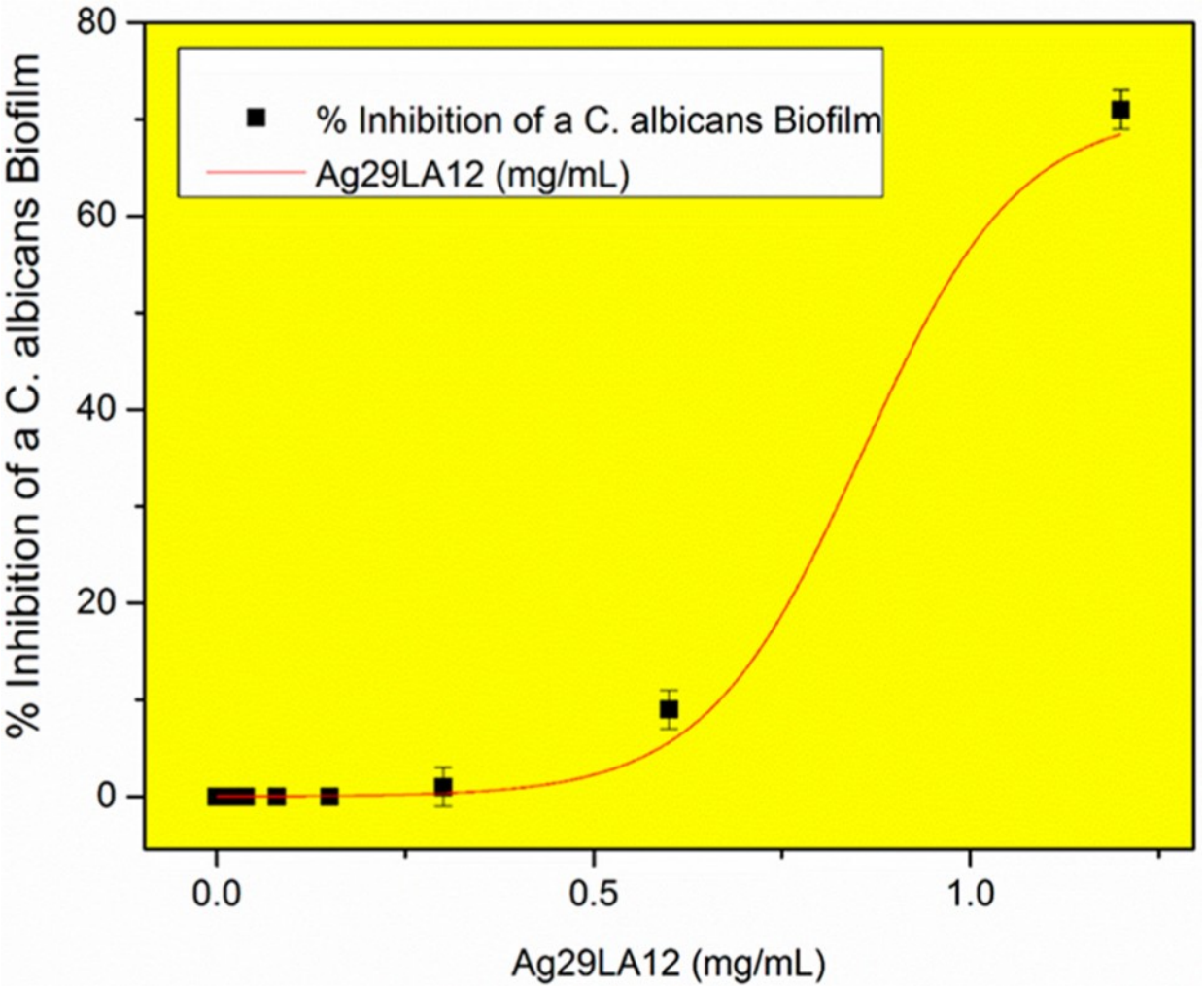

Figure 5.

$Ag_{29}LA_{12}$ cluster inhibits a *Candida albicans* biofilm at 0.94 mg Ag/mL half maximal inhibitory concentration IC50. Error bars represent + standard deviation from the mean.

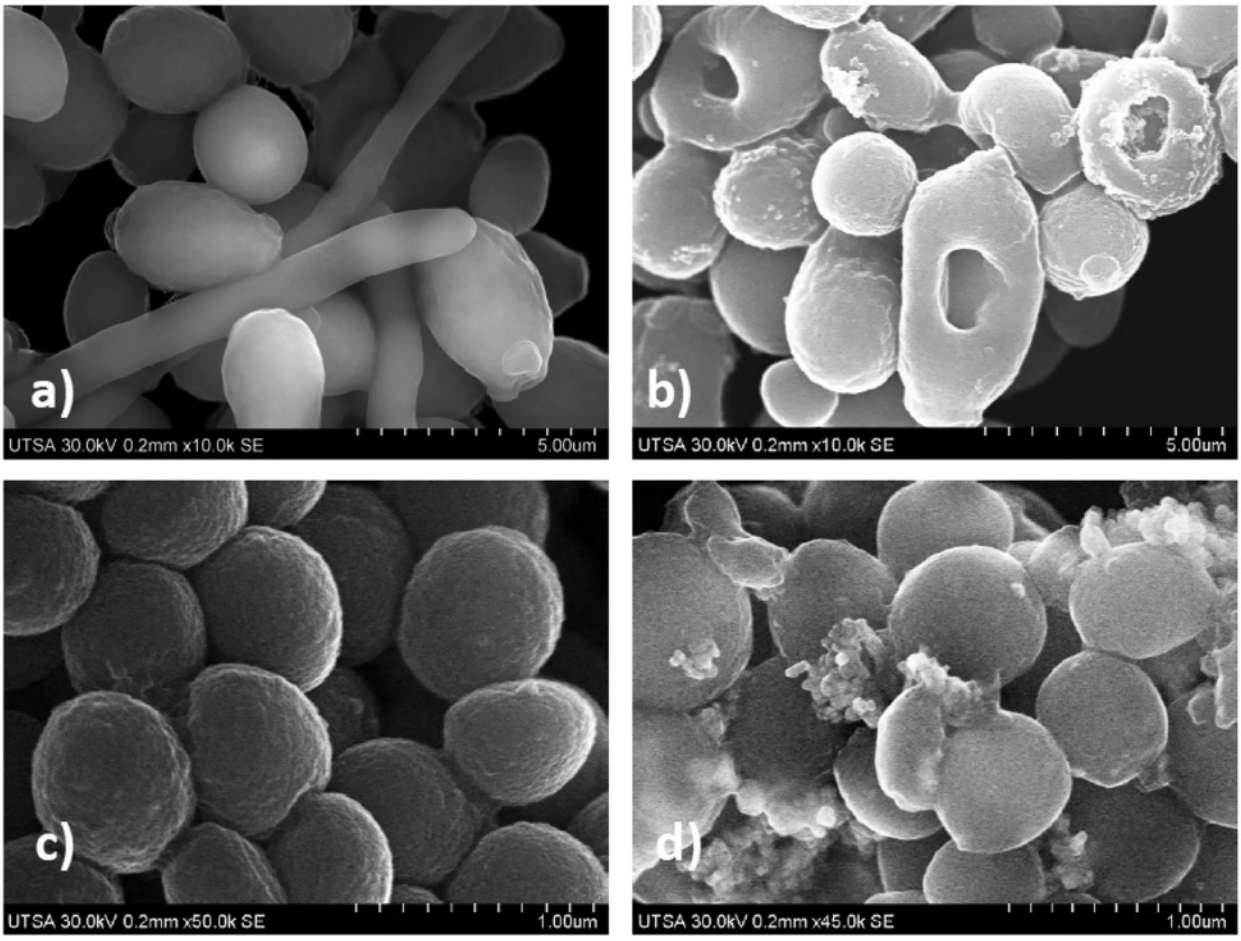

Figure 6.

(a, b) SEM images of a preformed biofilm of *Candida albicans*: (a) without treatment, displaying true hyphae and yeast cells displaying a smooth surface on the cell wall (CW) and a dense mesh-like network of yeasts cells and hyphal elements; and (b) after 24 h treatment of clusters at 0.94 mg-Ag/mL, showing the preformed biofilm of *Candida albicans* with scarce hyphae, and disrupted outer CW. Clusters becomes aggregated 24 h after incubation on the preformed biofilm, (c, d) SEM images of MRSA: c) MRSA cells without treatment; and (d) post-treatment, showings cell size and morphology changes of MRSA along with clusters interacting and agglomerated on the outer cell surface. Cluster concentration was 0.6 mg-Ag/mL for 24 h treatment.